remote sensing

MDPI

Article

Quasi-Biweekly Oscillation of $PM_{2.5}$ in Winter over North China and Its Leading Circulation Patterns

Xinsheng Zhu and Chenyu Yao *

Nanjing Institute of Environmental Science, Ministry of Ecology and Environment of the People's Republic of China, Nanjing 210042, China; zxs_dream@yeah.net
* Correspondence: cyyao1994@outlook.com

Abstract: Persistent pollution often occurs in North China in winter. The study of the sub-seasonal evolution characteristics of fine particles ($PM_{2.5}$) can provide a theoretical basis for the prediction and prevention of persistent pollution. Based on the high-resolution gridded data of $PM_{2.5}$ and NCEP/NCAR reanalysis, the sub-seasonal variation in $PM_{2.5}$ in North China in winter and its dominant circulation patterns from 1960/61 to 2019/20 were analyzed. The results show that, in winter, $PM_{2.5}$ in North China shows a dominant period of 10–20 days, and persistent heavy pollution occurs at the active phase of oscillation. Based on the $PM_{2.5}$ quasi-biweekly oscillation (QBWO) events, the 850 hPa wave train can be classified into four categories. It was found that, during the active phase of $PM_{2.5}$ QBWO, the wind speed is weak and humidity is high in the low-troposphere for all of the four event types, while the quasi-biweekly 850 hPa wave train and the track of geopotential height anomaly are significantly different. Based on the characteristics of circulation evolution, these four types of events can be named as eastward, split southward, southeastward, and merged event. The energy conversion between the basic flow and the quasi-biweekly disturbance, and the mean flow difference are responsible for the circulation diversity for different $PM_{2.5}$ QBWO events. The above research results can provide a theoretical basis for pollutant prediction.

Keywords: $PM_{2.5}$; quasi-biweekly oscillation; leading circulation patterns; K-means

Citation: Zhu, X.; Yao, C. Quasi-Biweekly Oscillation of $PM_{2.5}$ in Winter over North China and Its Leading Circulation Patterns. *Remote Sens.* **2023**, *15*, 4069. https://doi.org/10.3390/rs15164069

Academic Editor: Riccardo Buccolieri

Received: 28 June 2023
Revised: 10 August 2023
Accepted: 13 August 2023
Published: 17 August 2023

1. Introduction

A high concentration of fine particles ($PM_{2.5}$) pollution will cause significant negative impacts on the regional environment and human health, especially in densely populated and industrially developed cities [1]. Pollutant particles usually consist of primary particles and secondary particles [2]. Primary particles often include construction dust particles, straw and fossil fuel incineration. Secondary particles are mainly formed by various chemical reactions of the pollution components in the atmosphere under the influence of meteorological factors, which are difficult to remove under normal environmental conditions [2,3]. If they encounter heavy humidity and low wind, the probability of haze will increase. Compared with primary particles, the size of secondary particles is smaller, with a longer residence time in the atmosphere, longer transmission distance, longer duration, and stronger severity on human health and the atmospheric environment, and the harm of secondary pollutants is far greater than that of primary pollutants [4,5]. In general, the concentration of pollutants is determined by the emission source and meteorological conditions. Emission source has the greatest influence on the total amount of pollutants as a whole [6], and the meteorological conditions, for example, the wind in low troposphere, humidity, and the stability of the atmosphere, determine the regional transmission, sedimentation and generation of secondary pollutants [7,8]. Compared with primary sources, meteorological conditions have greater uncertainty and uncontrollable factors. The excessive concentration of pollutants is more likely to occur under special weather conditions conducive to the formation and accumulation of pollutants, such as

stable weather with a low wind speed, high humidity and less precipitation [9–11]. In January 2013, a severe haze occurred in Beijing, China, lasting for several days. Conducive weather conditions are an important ingredient of severe disasters, including reduced surface winter northerlies, weakened northwesterlies in the mid-troposphere, and enhanced thermal stability of the lower atmosphere [9,12]. Research by Cai et al. has also shown that, on the background of climate change, weather conditions will increase the frequency of severe haze occurrence in winter in Beijing, such as that occurring in 2013 [9].

North China is densely populated with rapid industrialization. As an important economic zone in eastern China, huge energy consumption and adverse atmospheric diffusion conditions have led to particularly serious $PM_{2.5}$ pollution in the region. In combination with the superimposed effects of the topography of the Taihang Mountains and Yanshan Mountains, some areas of North China are in a semi-enclosed terrain, which makes it more difficult for pollutants to diffuse [13]. There have been several polluted events with a $PM_{2.5}$ concentration of more than 500 $\mu g/m^3$, and the pollution often lasts for several days [12,14–16]. Research has shown that the weak weather system, low activity of strong cold air, extremely unfavorable local meteorological conditions, and geographical situation for pollutant diffusion in the Beijing–Tianjin–Hebei region of China in January 2013 were the external conditions that led to the formation of this severe haze pollution. The rapid conversion of gaseous pollutants into particles is an internal driving factor for the "explosive" and "persistent" nature of this strong haze pollution, especially the large amount of NOx, which is mainly emitted by fuel in the atmosphere, and promotes the rapid conversion of gaseous SO_2 from coal-fired emissions to particulate sulfate [17]. However, the serious pollution in February 2013 was related to the low wind speed near the surface, high humidity, and the stability of the boundary layer caused by temperature inversion [18]. As the aerosol is nearly saturated in the atmosphere, the sustainability of pollution depends on the diffusion characteristics of the atmospheric circulation to pollutants [19–24].

In terms of seasonal variation, the $PM_{2.5}$ concentration is highest in winter among the four seasons. This is mainly because, in winter, it is affected by coal-fired heating, which leads to a concentration of SO_2 that is significantly higher than in the other seasons. In addition, the temperature in winter is low, the pressure is high, the planetary boundary layer is low, turbulence and air convection are weak, and the temperature inversion phenomenon increases the stability of the atmosphere. Therefore, there are more occurrences of fine particle pollution events in winter [25,26].

In winter, the atmosphere in East Asia shows significant quasi-biweekly oscillation (QBWO) characteristics, including wind, temperature, and humidity [27,28]. The research shows that the temporal and spatial distribution of the $PM_{2.5}$ concentration in eastern China is closely related to the wave train in Eurasia [29–32]. Under the joint action of the polar front jet and the subtropical westerly jet, the quasi-biweekly evolutions of the Eurasian teleconnection pattern and Circum-global teleconnection pattern are responsible for the propagation of the wave trains, further affecting the quasi-biweekly evolution of $PM_{2.5}$ in eastern China [29]. The evolution of $PM_{2.5}$ in the Beijing–Tianjin–Hebei region is related to the QBWO of the East Asian trough, which can be traced back to the northwest of Eurasia [30]. It is worth noting that due to data limitations, the above studies were conducted from 2000 to 2019 [29] and from 2013 to 2017 [30]. However, over a longer period of time, the following questions remain: Is the concentration of $PM_{2.5}$ also characterized by QBWO? Does its leading circulation pattern have different characteristics in different years or decades?

In order to solve such scientific issues, this study intended to use $PM_{2.5}$ daily data to analyze the sub-seasonal characteristics of winter $PM_{2.5}$ in North China from 1960/61 to 2019/20, and explore the associated impact process of atmospheric QBWO. The rest of this paper is arranged as follows: The second part details the materials and methods, and the third part analyzes four types of leading circulation patterns and evolution mechanisms that affect the QBWO of $PM_{2.5}$; The fourth part includes the discussion.

2. Materials and Methods

2.1. Data

The $PM_{2.5}$ dataset used in this paper was from the regional $PM_{2.5}$ gridded data of China from 1960 to 2020 constructed by Zhong et al., with a horizontal resolution of $0.25^\circ \times 0.25^\circ$ and a temporal resolution of 6 h [33]. The data combine long-term visibility, conventional meteorological observations, emissions, and elevation. Additionally, a new feature engineering method that takes advantage of spatial features from 20 surrounding meteorological stations was employed to incorporate the spatial effects of the meteorological conditions. The 6-hourly $PM_{2.5}$ datasets from 1960 to 2020 are publicly accessible, and the gridded data are in the NETCDF format. These data are mainly used to analyze the distribution and evolution characteristics of $PM_{2.5}$.

Considering that the $PM_{2.5}$ data used in this study are reconstructed data, the observation of aerosol data was used to verify the research results. The aerosol data come from the AERONET (Aerosol Robotic Network), a global aerosol monitoring network jointly established by NASA (National Aeronautics and Space Administration) and LOA-PHOTONS (CNRS). The instrument operates at wavelengths of 340, 380, 440, 500, 675, 870, 940, and 1020 nm. The measurement of AERONET must be carried out under daytime and clear sky conditions, and the data need to be classified and screened according to certain standards, corresponding to three levels of data products, namely L1.0, L1.5, and L2.0. Among them, the L2.0 aerosol inversion products are data that have undergone cloud removal processing and manual inspection to ensure quality [34]. Considering the size and optical properties of $PM_{2.5}$ particles, as aerosol optical depth (AOD) mainly reflects the scattering and absorption characteristics of particles, the longer the wavelength, the lower the sensitivity to small particle scattering, while the sensitivity to large particle scattering increases. Therefore, longer wavelength AOD is more affected by large particles [35]. Consequently, in order to effectively avoid the influence of large particle sizes, the 440 nm band AOD is usually used to invert the $PM_{2.5}$ concentration, which has a strong correlation with the $PM_{2.5}$ concentration [36]. Considering the location and length of the observation data (>15 years), we selected the daily AOD Level 2.0 obtained at the 440 nm band in Beijing (39.977°N, 116.381°E) from 2001 to 2019 to compare with the gridded $PM_{2.5}$ concentration. The observed AOD data can be obtained online free of charge (https://aeronet.gsfc.nasa.gov/new_web/download_all_v3_aod.html (accessed on 1 June 2023))

To analyze the atmospheric circulation evolutions, the reanalysis data (from 1948–present) provided by National Centre for Environmental Prediction/National Centre for Atmospheric Research (NCEP/NCAR) were used in this study, including daily sea level pressure (SLP), 10 m wind, wind, geopotential height, relative humidity at pressure levels, with a horizonal resolution of $2.5^\circ \times 2.5^\circ$, and 17 pressure levels (1000, 925, 850, 700, 600, 500, 400, 300, 250, 200, 150, 100, 70, 50, 30, 20, 10 hPa) [37]. NCEP/NCAR data can be obtained online free of charge (https://psl.noaa.gov/data/gridded/data.ncep.reanalysis.html (accessed on 11 January 2023)) and are widely used in meteorological research.

This study focused on the winters from 1960/61 to 2019/20, representing a total of 60 winters. Here, winter includes the months from November to February of the next year (NDJF). AOD observation data of Beijing started in March 2001 and ended in March 2019, but the data for the winter of 2001/02 is missing, so we selected the AOD data for 17 winters (2002/03–2018/19) to evaluate some results of the gridded $PM_{2.5}$ data. If not particularly indicated, the conclusions drawn in this study are based on the results of winters over 60 years.

2.2. Method

This study selected North China (114–117°E, 35–40°N) with a high $PM_{2.5}$ concentration as the study area. The dominant period of the daily $PM_{2.5}$ in winter in North China was obtained by power spectrum analysis. A Butterworth bandpass filter was used to obtain the quasi-biweekly scale with the window of 10–20 days. When the peak value of 10–20-day

filtered $PM_{2.5}$ exceeded one standard deviation, the corresponding fluctuation was defined as a $PM_{2.5}$ QBWO event. Here, the peak day of quasi-biweekly $PM_{2.5}$ is defined as day 0; day n (n > 0) means n days after the peak day; and day −n means n days before the peak day.

Considering the influence of the quasi-biweekly evolution of atmospheric circulation on $PM_{2.5}$ QBWO events, this study selected the quasi-biweekly geopotential heights of 850 hPa on day −4 (4 days before the peak day), day −2 (2 days before the peak day) and day 0 (peak day) for K-means clustering to obtain the leading quasi-biweekly circulation. As a clustering analysis method, the essence of K-means clustering analysis is to gather the more similar and less different samples into one cluster according to the distance between samples to form multiple clusters [38]. The samples within the same cluster have high similarity, but the samples between different clusters have strong differences. The K-means clustering method has been widely used in the analysis of the dominant circulation pattern of atmospheric circulation [39,40].

In this study, the morphology and propagation characteristics of the Rossby wave train are characterized by calculating the wave activity flux (WAF). The horizontal WAF is as follows [41,42]:

$$W = \frac{p\cos\phi}{2|\mathrm{U}|}\begin{pmatrix} \frac{u}{a^2\cos^2\phi}\left[\left(\frac{\partial\psi'}{\partial\lambda}\right)^2 - \psi'\frac{\partial^2\psi'}{\partial\lambda^2}\right] + \frac{v}{a^2\cos\phi}\left[\frac{\partial\psi'}{\partial\lambda}\frac{\partial\psi'}{\partial\phi} - \psi'\frac{\partial^2\psi'}{\partial\lambda\partial\phi}\right] \\ \frac{u}{a^2\cos\phi}\left[\frac{\partial\psi'}{\partial\lambda}\frac{\partial\psi'}{\partial\phi} - \psi'\frac{\partial^2\psi'}{\partial\lambda\partial\phi}\right] + \frac{v}{a^2}\left[\left(\frac{\partial\psi'}{\partial\phi}\right)^2 - \psi'\frac{\partial^2\psi'}{\partial\phi^2}\right] \end{pmatrix} \quad (1)$$

where 'ψ' is a quasi-biweekly stream function, $\mathrm{U} = (u, \mathrm{v})$ represents the average climatic circulation field. u, v represent the zonal and meridional wind, and a represents the radius of the Earth. p is the pressure.

The barotropic energy conversion process is based on the theory of Cai et al. [43], and the barotropic energy conversion formula between the kinetic energy of a quasi-biweekly scale disturbance and the basic airflow is as follows:

$$C_k = \frac{1}{2}(v'^2 - u'^2)\left(\frac{\partial\overline{u}}{\partial x} - \frac{\partial\overline{v}}{\partial y}\right) - u'v'\left(\frac{\partial\overline{v}}{\partial x} + \frac{\partial\overline{u}}{\partial y}\right) \quad (2)$$

where u and v represent the zonal and meridional components of the horizontal wind speed, the variable with an apostrophe indicates a quasi-biweekly scale, and the overbar indicates the mean flow. When $C_k > 0$, it indicates that the mean kinetic energy is converted into quasi-biweekly scale disturbance kinetic energy, and vice versa, it indicates that the disturbance releases kinetic energy and converts it into mean kinetic energy.

3. Results

3.1. The Spatial Distribution and Quasi-Biweekly Evolution Characteristics of $PM_{2.5}$ Concentration in North China in Winter

Firstly, the spatial distribution of $PM_{2.5}$ in winter (NDJF) in China was analyzed (Figure 1a). It shows that North China is a significant high-value region, and the average $PM_{2.5}$ concentration in winter is more than 120 $\mu g/m^3$, as shown in the red box in Figure 1a (114–117°N, 35–40°E). Therefore, the region in the red box was selected as the key region to study the $PM_{2.5}$ in North China. The daily standard deviation was used to express its variation intensity, and it was found that the value exceeds 40 $\mu g/m^3$ in North China. Further analysis of the dominant period of $PM_{2.5}$ concentration in North China was carried out by power spectrum method (Figure 1b). It was found that, in addition to the synoptic scale (<10 d) disturbance, the power spectral density (real line in Figure 1b) has obvious peaks at 10–20 days, and passes the red noise test of 95% (dashed line in Figure 1b). This shows that, on the sub-seasonal scale, the $PM_{2.5}$ concentration mainly presents a quasi-biweekly (10–20 days) scale oscillation. According to the method in Section 2, 168 typical $PM_{2.5}$ QBWO events were selected in North China, with an average of approximately 2–3 times per winter. Figure 1c shows the frequency of $PM_{2.5}$-QBWO events each winter

from 1960/61 to 2019/20. It shows that the lowest frequency occurred in the 1960s, when the average concentration of $PM_{2.5}$ in winter was lower than 80 μg/m^3. After the 1970s, it gradually increased, and from 2014, it showed a weakening trend. AOD in Beijing (the red line in Figure 1c) has a strong correlation with the average $PM_{2.5}$ concentration in North China, with a correlation coefficient of 0.693, reaching a 99.9% confidence test. From the evolution of AOD from 2002/03 to 2018/19, it can also be concluded that, after 2014, the AOD value in Beijing entered a weakening stage.

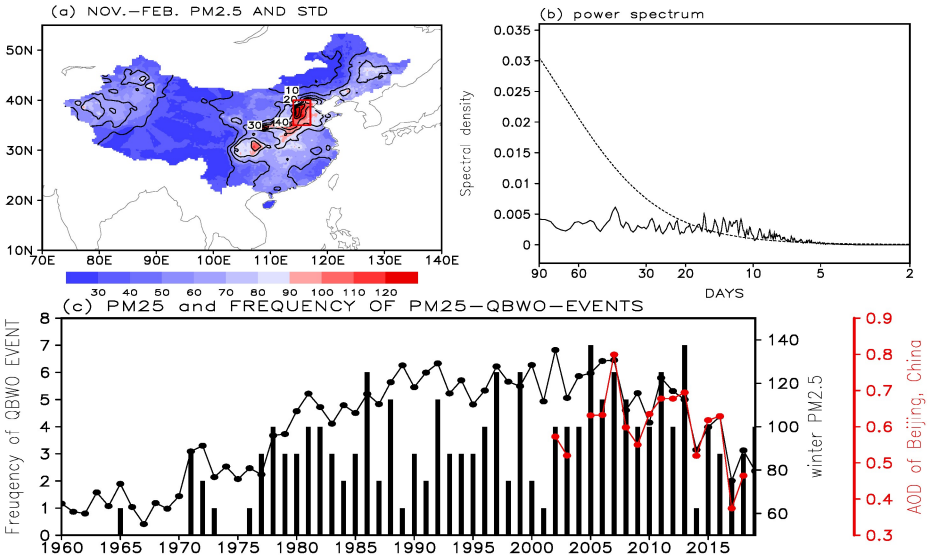

Figure 1. (**a**): Winter mean $PM_{2.5}$ concentration (shadow) and its standard deviation (contour), unit: μg/m^3, red box for North China (114–117°E, 35–40°N). (**b**): Power spectrum analysis of $PM_{2.5}$ concentration in North China (solid line is power spectrum density, and dotted line is 95% red noise test). (**c**): $PM_{2.5}$ concentration (black curve, right coordinate axis in black, unit: μg/m^3), frequency of $PM_{2.5}$ QBWO events (column, left coordinate axis, unit: times) in North China in the winter from 1960/61 to 2019/20 and AOD of Beijing from 2002/03 to 2018/19 (red curve, right coordinate axis in red).

According to the synthetic analysis of 168 $PM_{2.5}$ QBWO events, it was found that on the peak day of the oscillation event (Figure 2a), the concentration of $PM_{2.5}$ in North China can even reach 270 μg/m^3, and the pollution is serious. The quasi-biweekly anomaly of $PM_{2.5}$ exceeds 50 μg/m^3. Taking the peak day of $PM_{2.5}$ QBWO events as day 0, the evolution of $PM_{2.5}$ and the quasi-biweekly $PM_{2.5}$ from day −10 to day 10 are shown in Figure 2b. The evolution characteristics of $PM_{2.5}$ are the same as those of the quasi-biweekly $PM_{2.5}$. On day −6 or day 6, the concentration of $PM_{2.5}$ is less than 100 μg/m^3, and on the peak day, the average concentration of $PM_{2.5}$ in North China is more than 180 μg/m^3. From day −3 to day 3, the concentration of $PM_{2.5}$ is more than 140 μg/m^3, so it can be considered that significant and continuous pollution occurs in the active phase of QBWO.

Further analysis was conducted on the evolution of AOD during $PM_{2.5}$ QBWO. Based on the synthesis of 66 $PM_{2.5}$ QBWO events in the winter of 2002/03–2018/19, it was found that the daily evolution characteristics of AOD in Beijing are consistent with the $PM_{2.5}$ in North China. In the active phase of $PM_{2.5}$ QBWO, the value of AOD is large, while in the inactive phase, the value of AOD is small, which further verifies the credibility of the $PM_{2.5}$ gridded data.

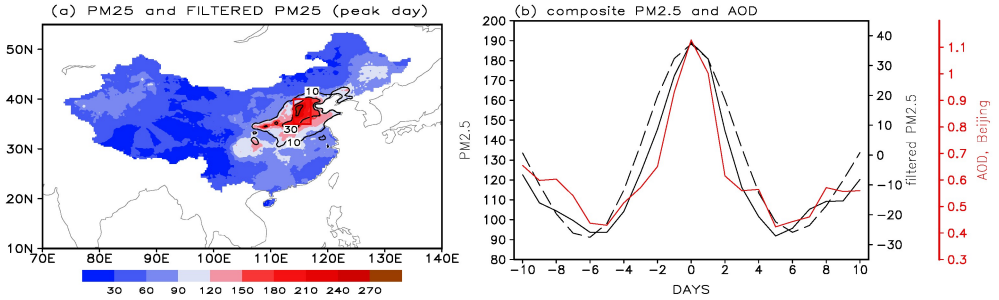

Figure 2. (**a**): Composite $PM_{2.5}$ concentration (shadow) and 10–20-day filtered $PM_{2.5}$ concentration (contour) on the peak day based on the 168 QBWO event of $PM_{2.5}$, unit: $\mu g/m^3$, red box for North China. (**b**): Synthesis of the regional average $PM_{2.5}$ (black line, left coordinate axis) and 10–20-day filtered $PM_{2.5}$ (black dashed line, right coordinate axis in black) in North China (unit: $\mu g/m^3$) based on 168 events from 1960/61 to 2019/20 and AOD in Beijing (right coordinate axis in red) based on 66 events from 2002/03 to 2018/19.

Further analysis was conducted on the circulation characteristics corresponding to the QBWO of $PM_{2.5}$. First, the oscillation is divided into two stages: the pollution active period (day −3 to day 3) and the pollution interruption period (day −6 to −4 and day 4 to 6). Figure 3a shows the SLP on the peak day and the SLP difference between the active and interrupted periods of $PM_{2.5}$ QBWO. On the peak day of the QBWO events, Mongolia is controlled by the Mongolian high and North China is in front of the Mongolian high. Comparing the SLP during the active period and the interrupted period of $PM_{2.5}$ QBWO, it can be seen that during the active period, a positive anomaly of SLP occurs in the northwest of the Mongolia high. The eastern part of China is controlled by an abnormal low-pressure system. When the wind velocity of the surface layer is weak, it is generally not conducive to the diffusion of pollutants, so the characteristics of 10 m wind velocity were further analyzed (Figure 3b). This shows that the average wind speed on land is significantly weaker than that on the sea on the peak day, which may be due to the greater friction on land. In the active period of $PM_{2.5}$ QBWO, the wind from eastern China to offshore areas is weaker than that in the interrupted period. During the active period of $PM_{2.5}$ oscillation, eastern China is located in front of the quasi-biweekly abnormal low pressure. The intensity of the quasi-biweekly abnormal low pressure is close to the that of the unfiltered anomaly, and it shows a significant southerly anomaly (Figure 3c), which weakens the northerly wind. At the same time, quasi-biweekly humidity and wind at 850 hPa (Figure 3d) were analyzed. During the active period of $PM_{2.5}$ QBWO, more water vapor is transported to North China due to the anomalies of southwest wind and southeast wind, and the relative humidity in eastern China is higher than that during the inactive period. The difference in quasi-biweekly geopotential height between the active period of $PM_{2.5}$ QBWO and the interrupted period shows that the wave train at 850 hPa is clearer than that at the surface layer. A clear quasi-biweekly wave train extends from the Ural Mountains to East Asia (Figure 3e). The quasi-biweekly geopotential height of 300 hPa and 850 hPa show a similar wave train distribution (Figure 3f), and geopotential anomaly from the Caspian Sea to the Pacific Ocean present the distribution of "-+-".

3.2. Circulation Classification of $PM_{2.5}$ QBWO Events

The research shows that the circulation pattern is diverse when haze occurs [23,44,45]. However, the characteristics of the leading circulation pattern affecting the $PM_{2.5}$ QBWO are not clear. Therefore, for 168 $PM_{2.5}$ QBWO events, taking into account the mobility of the weather system, the circulation classification is carried out based on the evolution of 850 hPa quasi-biweekly geopotential height using the K-means clustering method in Section 2. The results are shown in Figure 4. The frequency of the four types of events is 51, 52, 43 and 22, respectively.

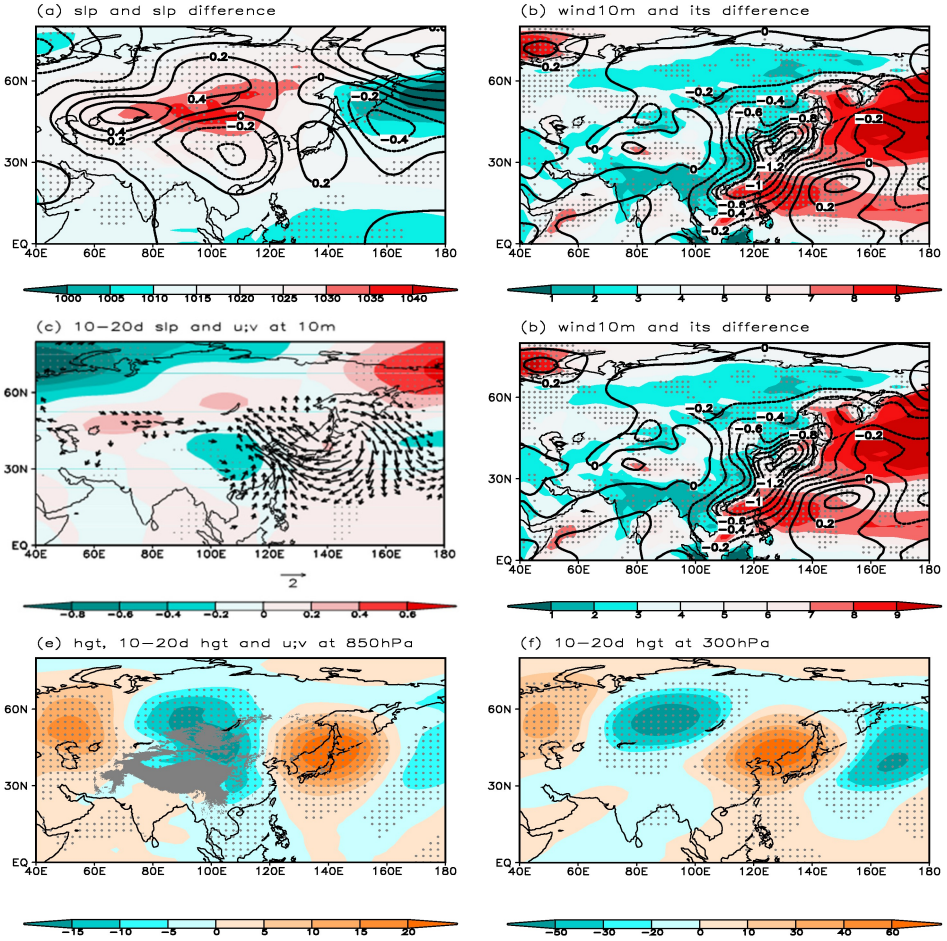

Figure 3. (**a**): SLP (color shadow) on the peak day of $PM_{2.5}$ QBWO and the SLP difference (unfiltered, contour) between the active period and interrupted periods of $PM_{2.5}$ oscillation, unit: hPa. (**b**): Same as (**a**), but represents 10 m wind velocity, unit: m/s. (**c**): Quasi-biweekly SLP (color shadow, unit: hPa) and 10 m wind velocity (vector, unit: m/s) difference between the active period and interrupted periods of $PM_{2.5}$ QBWO. (**d**) Quasi-biweekly relative humidity (color shadow, unit: %) and wind velocity (vector, unit: m/s) difference at 850 hPa between the active period and interrupted periods of $PM_{2.5}$ QBI. (**e**) Quasi-biweekly geopotential height (color shadow, unit: gpm) at 850 hPa between the active period and interrupted periods of $PM_{2.5}$ QBWO. (**f**): SI as (**e**), but for 300 hPa. The dots in a–f indicate that the difference in SLP, 10 m wind speed, 10–20-day filtered SLP, 10–20-day filtered relative humidity, and 10–20-day filtered 850 and 300 hPa geopotential heights between the active and interrupted periods of $PM_{2.5}$ QBWO pass the 95% *t*-test.

For $PM_{2.5}$-QBWO1 (the first type leading pattern) Figure 4(a1–c1), at day −4, the Ural Mountains is controlled by an abnormally low-pressure system, and there is an abnormal anti-cyclone in front of Baikal Lake and an abnormal cyclone in Kuril Islands. After that, the wave train moves eastward. On day 0, the Baikal Lake area is controlled by a quasi-biweekly cyclone, and Japan is controlled by an anti-cyclone.

For $PM_{2.5}$-QBWO2 (the second type of event) Figure 4(a2–c2), on day −4, the area from Nova Zembla to the Ural Mountains is controlled by a quasi-biweekly cyclone, the area south of Baikal Lake is controlled by an anti-cyclone, and the area from northern Japan to the Kamchatka Peninsula is controlled by an abnormal cyclone; On day −2, the intensity of the cyclone near Nova Zembla increases, and the scope expands to Baikal Lake; On day 0, the cyclone near Nova Zembla continues to spread in the southeast, and North China is in front of the cyclone and behind the anti-cyclone.

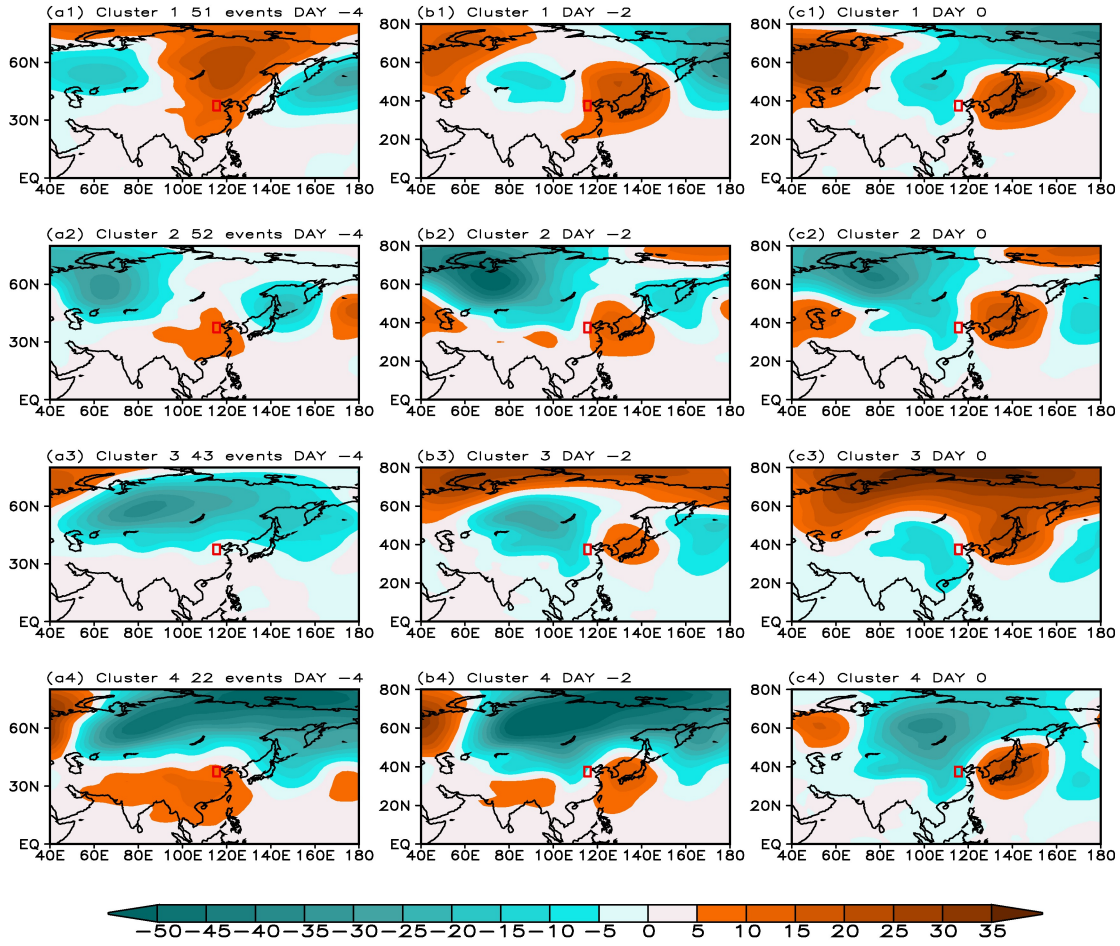

Figure 4. 850 hPa quasi-biweekly geopotential height obtained by K-means cluster analysis. (**a1**,**b1**,**c1**) represent day −4, day −2, and day 0 of $PM_{2.5}$-QBWO1. (**a2**,**b2**,**c2**), (**a3**,**b3**,**c3**), and (**a4**,**b4**,**c4**) are the same as (**a1**,**b1**,**c1**), but represent $PM_{2.5}$-QBWO2, $PM_{2.5}$-QBWO3 and $PM_{2.5}$-QBWO4, respectively. Unit: gpm. The red box indicates North China.

For $PM_{2.5}$-QBWO3 (the third type of event) Figure 4(a3–c3), on day −4, the area from the Ural Mountains to the Far East is controlled by a zonal distributed cyclone; on day −2, the high-latitude region is controlled by an anti-cyclonic anomaly, the area from Balkash Lake to Baikal Lake is still controlled by a cyclone and the area from Japan to South Korea is controlled by an abnormal anti-cyclone; on day 0, the cyclone moves southward, and the whole mid–high latitude area is controlled by an abnormal anti-cyclone.

For $PM_{2.5}$-QBWO4 (the fourth type) Figure 4(a4–c4), on day −4, the front of the Ural Mountains to the Pacific Ocean are controlled by an abnormal cyclone, and the south of 40°N is controlled by an anti-cyclone; on day −2, the intensity of cyclone in the mid–high latitudes increases and expands southward; on day 0, the abnormal cyclone expands southward to South China, and Japan and South Korea are controlled by an anti-cyclone.

From the above analysis, it can be seen that, on the peak day of $PM_{2.5}$ QBWO, North China is located in front of the cyclone and behind the anti-cyclone, but the circulation evolutions of the four kinds of events show great differences.

The interannual variation and interdecadal difference in the frequency of the four types of $PM_{2.5}$ QBWO events are shown in Figure 5. The results show that frequency of $PM_{2.5}$-QBWO1 presented an increasing trend after 2000, with the highest frequency of 5 in the winter of 2013/14 (Figure 5a). The frequency in the 2000s and 2010s was higher than that of other three categories. $PM_{2.5}$-QBWO2 rarely occurred in the 1980s, and the frequency of such events was highest in the winter of 2005/06 and the winter of 2019/20. It is worth noting that the $PM_{2.5}$ oscillation events in the 1970s were mainly $PM_{2.5}$-QBWO2, and the

frequency in the 1990s was also higher than that of other types of events (Figure 5b,e). $PM_{2.5}$-QBWO3 occurred most in the 1980s, and the highest frequency was 4 in the winter of 1986/87; the frequency was slightly lower than that of $PM_{2.5}$-QBWO1 in the 2000s (Figure 5c,e). $PM_{2.5}$-QBWO4 occurred more frequently in the 1980s and there was only one event after the 2010s (Figure 5d,e).

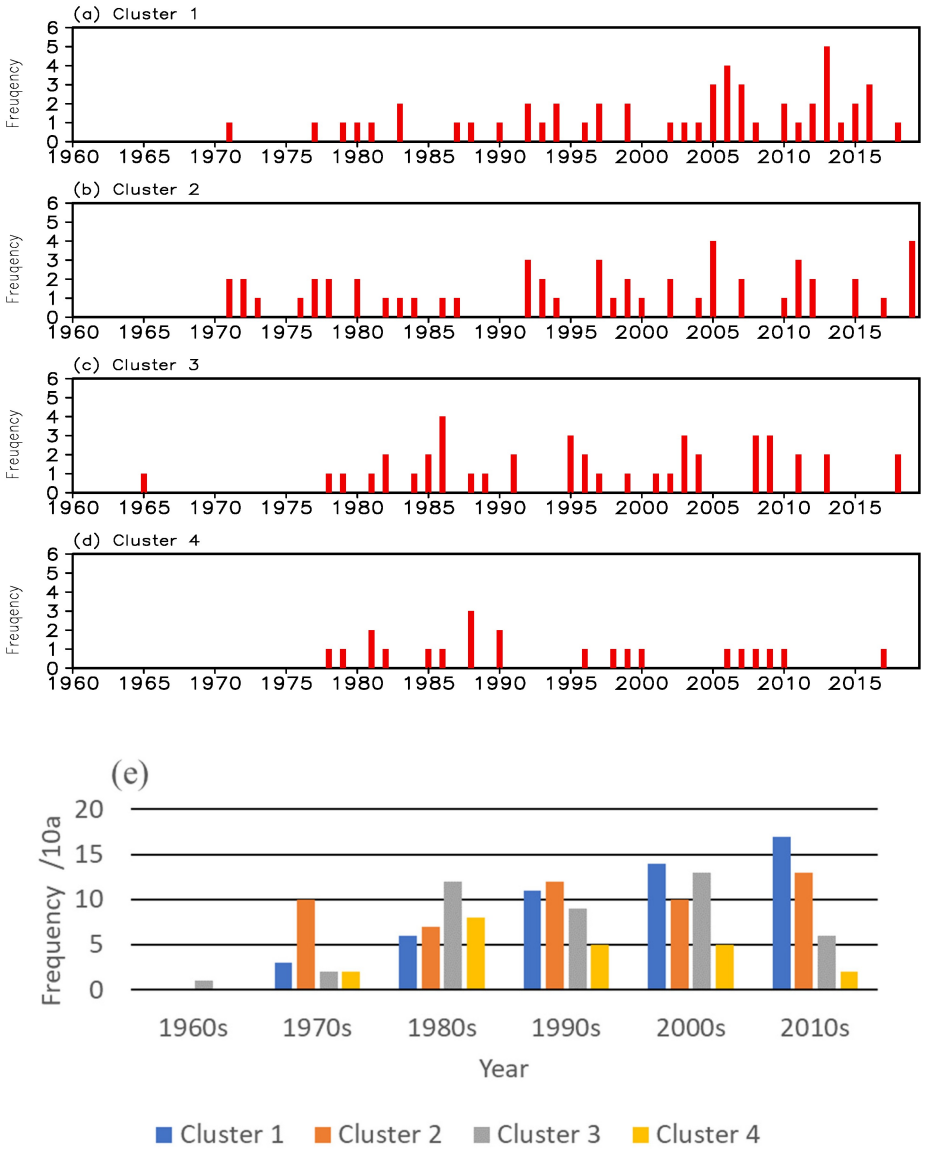

Figure 5. The frequency of four types of events in the winter from 1960/61 to 2019/20. (**a**–**d**) represent the first to fourth categories ($PM_{2.5}$-QBWO1, 2, 3, 4) (unit, times/year). (**e**) shows the frequency of four types of events in different decades (times/10 years).

3.3. Quasi-Biweekly Circulation Evolution of Four Kinds of $PM_{2.5}$ QBWO Events

Figure 6 shows the evolution of quasi-biweekly $PM_{2.5}$, the geopotential height and relative humidity at 850 hPa, and the near-surface wind speed of four types of events. First of all, among the four categories of $PM_{2.5}$ QBWO events, there is no significant difference in the quasi-biweekly $PM_{2.5}$ amplitude in the key areas, and $PM_{2.5}$ in $PM_{2.5}$-QBWO4 is slightly stronger than the other three categories. A weak 10 m wind speed and strong relative humidity correspond with strong a $PM_{2.5}$ concentration, where the extremely weak wind speed is approximately two days ahead of the extremely high value of $PM_{2.5}$, while the peak value of relative humidity is 1–2 days behind the peak value of $PM_{2.5}$. For $PM_{2.5}$-QBWO1 (Figure 6a), the quasi-biweekly geopotential height anomaly in the key area

is positive before day 0, and after the peak day, the key area turns to a negative anomaly. For $PM_{2.5}$-QBWO2 (Figure 6b), the quasi-biweekly geopotential height anomaly is positive from day −8 to day −2 and negative from day −1 to day 4. The geopotential height anomaly in $PM_{2.5}$-QBWO3 (Figure 6c) is not obvious, and it is negative from day −5 to day 2. For $PM_{2.5}$-QBWO4 (Figure 6d), the key area is always controlled by the negative geopotential highly anomaly from day −3 to day 4. It can be seen that there are significant differences in the quasi-biweekly geopotential height evolution of the four types of events. Therefore, the spatial distribution and propagation characteristics of 10–20-day filtered geopotential height were further analyzed.

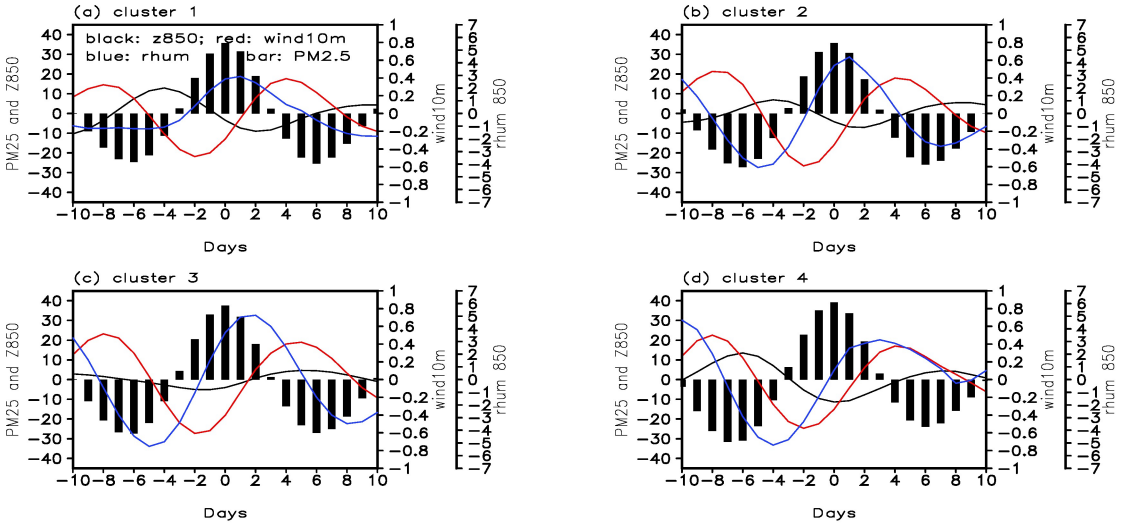

Figure 6. The composite spatial average quasi-biweekly $PM_{2.5}$ (histogram, unit: $\mu g/m^3$), 10 m wind speed (red solid line, unit: m/s), 850 hPa geopotential height (black solid line, unit: gpm), and 850 hPa relative humidity (blue solid line, unit: %) in North China. (**a**–**d**) represent $PM_{2.5}$-QBWO1–4, respectively.

Considering that the dominant period of $PM_{2.5}$ QBWO event is approximately 13 days, Figure 7 shows the composite of the quasi-biweekly wave action flux (WAF, vector), the geopotential height anomaly (shaded), and its tendency (contour) at 850 hPa from day −6 to day 6. For $PM_{2.5}$-QBWO1, the results show that during the period of day −6 to day −4, Figure 7(a1,a2), the quasi-biweekly cyclone is located near the Ural Mountains, with a negative geopotential tendency in front of the cyclone, and an abnormal anti-cyclone in the Baikal Lake area, with a positive tendency to the east. Therefore, the fluctuation propagates eastward. From day −2 to day 0, Figure 7(a3,a4), guided by the negative geopotential tendency, the low-pressure system moves from the west side of Baikal Lake to the vicinity of Baikal Lake. At this time, North China is located in front of the cyclone and behind the anti-cyclone. The anomalous cyclone then continues to move eastward. As its overall propagation path is mainly eastward, the $PM_{2.5}$-QBWO1 event can also be called the eastward propagation (EP) event. From day −6 to day −4, WAF propagates eastward from the Urals Mountains and westward from the Pacific Ocean near 60°N. In addition, WAF propagates southeastward in front of Baikal Lake.

The quasi-biweekly cyclone for the $PM_{2.5}$-QBWO2 event is located near the Caspian Sea on day −6 (Figure 7(b1)). Subsequently, guided by the negative geopotential tendency, it develops northward and increases in intensity, reaching its maximum on day −2, Figure 7(b2,b3). The intensity of the anomalous cyclone weakens slightly, and the scope expands, extending southward in China on day 0, Figure 7(b4). On day 2, the low-pressure center at mid–high latitudes weakens and moves eastward, splitting a center in southern China. Therefore, the $PM_{2.5}$-QBWO2 event can be named as an eastward propagation and splitting (EP-S) event. WAF near 60°N of the EP-S events is stronger than that of the EP events.

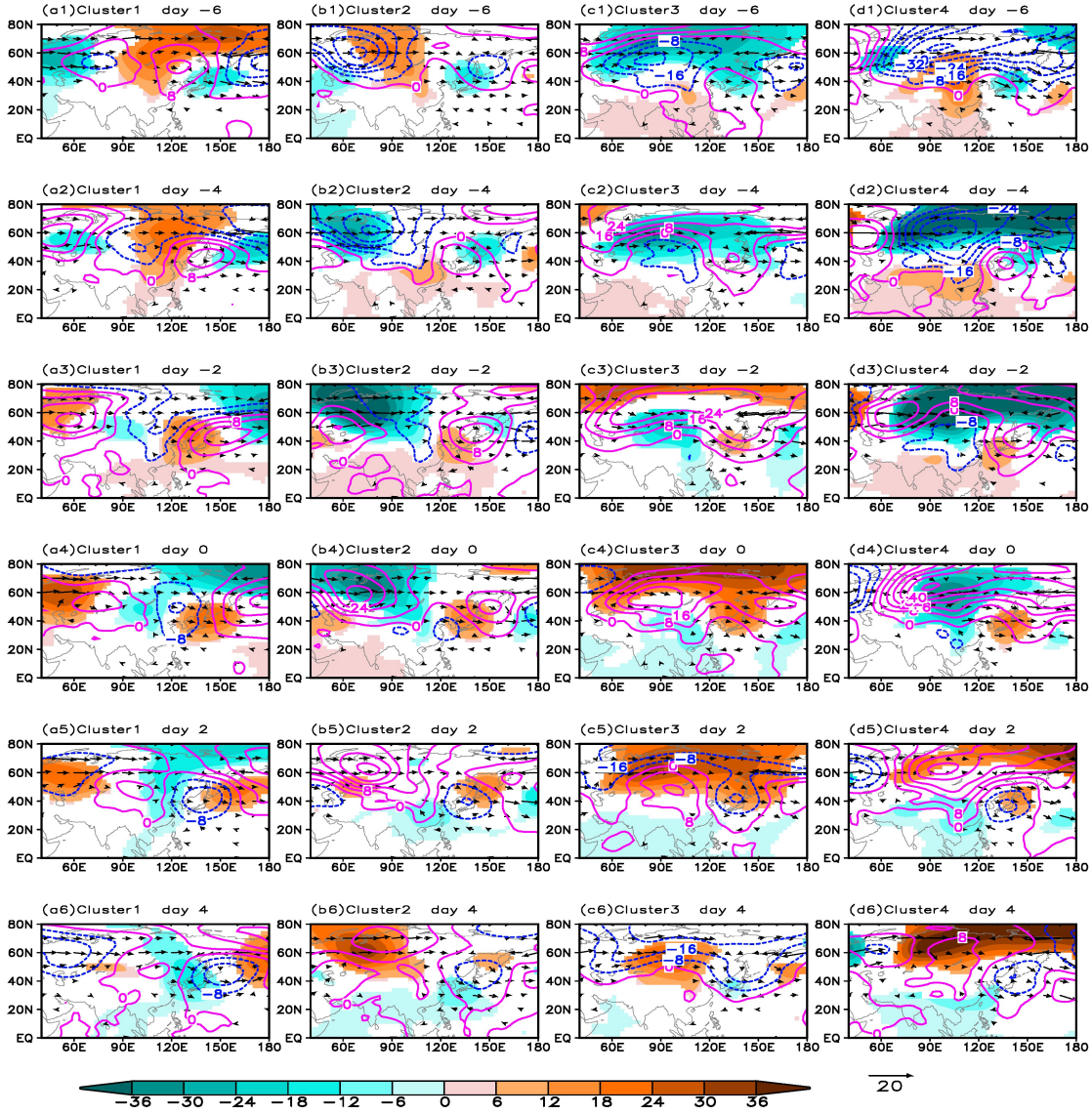

Figure 7. The synthesized quasi-biweekly geopotential height at 850 hPa (shadow, only the area that has passed the significance test is plotted, unit: gpm) and its tendency (contour, unit: gpm d^{-1}), and wave action flux (vector, unit: m^2 s^{-2}). (**a1**–**a6**) represent day −6 to day 4 for $PM_{2.5}$-QBWO1 event, with an interval of 2 days. (**b1**–**b6**), (**c1**–**c6**), and (**d1**–**d6**) are the same as (**a1**–**a6**), but represent the second, third, and fourth categories of events, respectively.

The $PM_{2.5}$-QBWO3 event can be referred to as the southeastward propagation (SEP) type. On day −6, north of Baikal Lake is under the control of a quasi-biweekly cyclone, and the geopotential tendency in Baikal Lake is negative, leading the quasi-biweekly cyclone to move from the west of Baikal Lake to the south Figure 7(c1–c3). At this time, the mid–high latitudes are under the control of a strong positive geopotential tendency, and the high latitudes are gradually controlled by the anti-cyclone, with the cyclone weakening while moving to the south Figure 7(c4). From day 2 to day 4, the anti-cyclone at mid–high latitudes moves southward Figure 7(c4,c5). Therefore, the SEP event is characterized by the transmission and weakening of the weather system from the polar regions to the southeast. The WAF of the SEP events is mainly concentrated around 60°N.

The quasi-biweekly cyclones of the $PM_{2.5}$-QBWO4 event are located near the Ural Mountains and East Siberia on day −6, and there is a strongly negative geopotential tendency in the north of Baikal Figure 7(d1), causing the two cyclones to gradually merge Figure 7(d2,d3). Subsequently, the entire high-latitude region is controlled by a positive

tendency of geopotential height, and the south of Lake Baikal is controlled by a negative tendency, which weakens the low pressure and moves southward Figure 7(d3,d4). Therefore, the $PM_{2.5}$-QBWO4 event is called a combined southward propagation (CSP) event. From day 2 to day 4, the cyclone moves eastward under the guidance of the negative tendency on the east side Figure 7(d5,d6). In the CSP events, the WAF propagating from East Siberia to the west near 60°N is significantly stronger than that of the other event types.

Figure 8 shows the evolution of the 300 hPa geopotential height during the active pollution period (day −2 to day 2) of the $PM_{2.5}$ QBWO. The QBWO intensity of the geopotential height at 300 hPa is significantly stronger than that at 850 hPa. The $PM_{2.5}$-QBWO1 events show a significant eastward propagation, accompanied by an increase in intensity (Figure 8a,e,i). The position of the 500 hPa quasi-biweekly cyclone (blue triangle in Figure 8) is close to that at 300 hPa, while the position of the 850 hPa quasi-biweekly cyclone center (red triangle) is slightly east by south, indicating the feature of the system tilting westward with height. The $PM_{2.5}$-QBWO2 events exhibit a significant southeastward movement and weakened intensity at 300 hPa, with the quasi-biweekly cyclone center position overlapping at different pressure levels. On day 2, the weak cyclone at 300 hPa is located in the west of Baikal Lake, and the 850 hPa cyclone is located in South China (Figure 8b,f,j), which means that quasi-biweekly cyclone in the upper troposphere only propagates eastward and does not split into two centers. The $PM_{2.5}$-QBWO3 events exhibit southeastward propagating characteristics at 300 hPa (Figure 8c,g,k), with a slight decrease in intensity. There is a significant difference in the location of the 850 hPa cyclone and the 300 hPa cyclone. The cyclone at 850 hPa is always located on the southeast side of that at 300 hPa, and its inclination with altitude is significantly stronger than the $PM_{2.5}$-QBWO1 event. The $PM_{2.5}$-QBWO4 events exhibit the characteristics of eastward and westward transmission converging at 300 hPa, which is similar to that at 850 hPa. The location of the 850 hPa low-pressure center coincides with the upper level at high latitudes, but on day 2, the 850 hPa quasi-biweekly low-pressure center quickly moves to southern China (Figure 8d,h,i). To sum up, the wave train propagation characteristics at different pressure levels are similar. However, only in the lower troposphere, can quasi-biweekly cyclones reach South China.

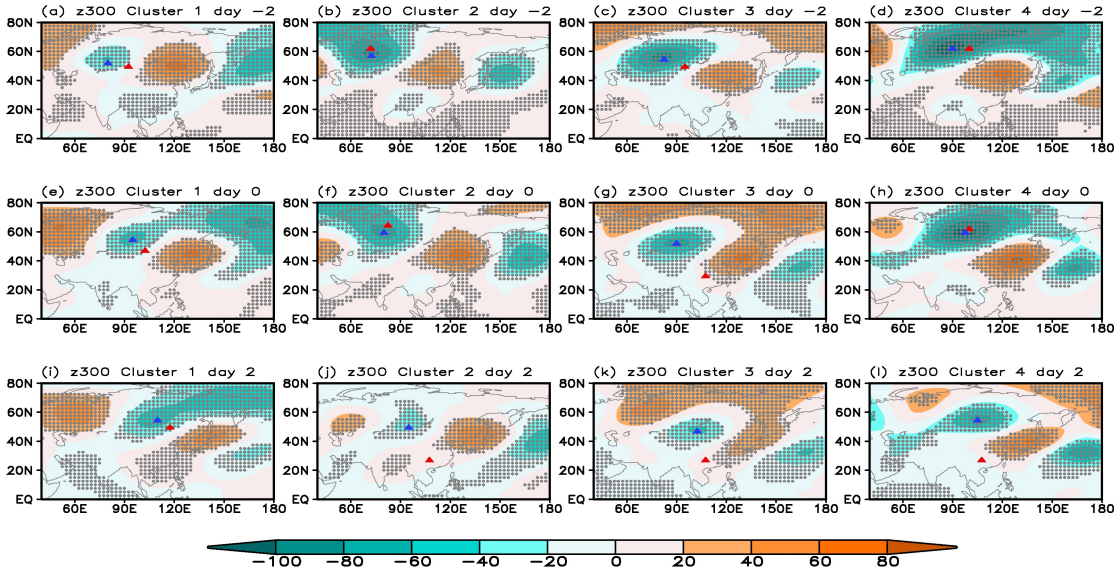

Figure 8. The synthesis of quasi-Biweekly geopotential height (unit: gpm). (**a**,**e**,**i**) represent $PM_{2.5}$-QBWO1 events; (**b**,**f**,**j**) represent $PM_{2.5}$-QBWO2 events; (**c**,**g**,**k**) represent $PM_{2.5}$-QBWO3 events; (**d**,**h**,**l**) represent $PM_{2.5}$-QBWO4 events. The red triangles indicate the center position of the abnormal cyclone at 850 hPa, and the blue triangle indicates the center position of the abnormal cyclone at 500 hPa. The dotted area indicates that the 95% confidence test has been passed.

3.4. The Propagation Mechanism of Quasi-Biweekly Geopotential Height for the $PM_{2.5}$-QBWO Events

The propagation and development of Rossby waves are generally related to the basic flow and energy conversion of different scale systems [46,47]. Firstly, the climatic basic flow at 850 hPa was analyzed, and the energy conversion process between the basic flow and quasi-biweekly scale disturbances was diagnosed, as shown in Figure 9. At 850 hPa (Figure 9a), the basic flow in the mid-latitude of the Asian continent is dominated by westerly winds, while in East Asia, it is controlled by northwest winds, and the north wind can reach around 30°N. In the North Pacific Ocean, there is an obvious cyclonic circulation near the Kamchatka Peninsula (the Aleutian Low). In the north of the Aleutian Low is an easterly wind, converging with the westerly wind of the Asian continent on the east coast of East Asia, and then turning into northerly winds. The barotropic energy conversion near Aleutian is the strongest, mainly from basic flow to quasi-biweekly scale disturbances. It is worth noting that there is a positive barotropic energy conversion center in southern China at 850 hPa, which is conducive to the development of quasi-biweekly disturbances. The basic airflow at 300 hPa (Figure 9b) is mainly characterized by westerly winds, with the strongest westerly winds located near 30°N, while the influence of northerly winds mainly stays north of 40°N. In addition, the strongest positive barotropic energy conversion occurs on the ocean surface in eastern Japan, while there is no significant energy conversion in southern China. Based on the diagnosis of basic airflow and barotropic energy conversion, it can be concluded that the quasi-biweekly cyclone in the lower troposphere can propagate southward to lower latitudes, mainly due to two aspects: one is that the mean meridional flow in the lower troposphere is stronger than that in the upper troposphere, and the other is that quasi-biweekly disturbances in South China can obtain energy from basic airflow, thereby enabling the development of disturbances.

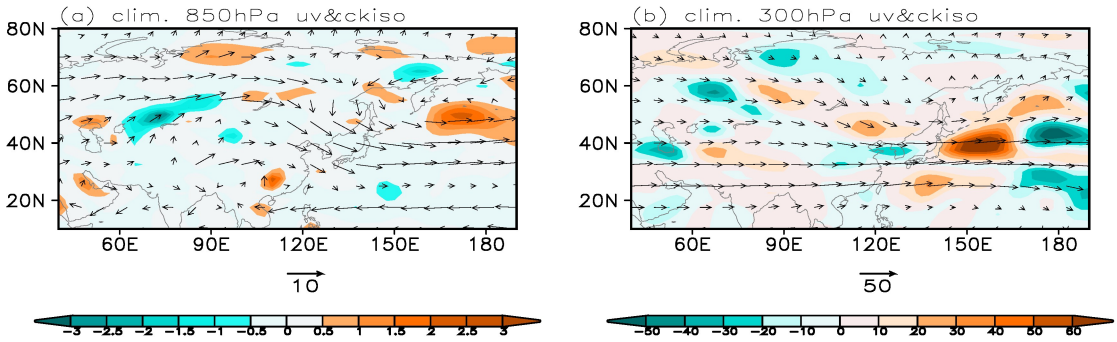

Figure 9. The average winter wind (vector, unit: m/s) and barotropic energy conversion (color shadow, unit: m^2/s^3) of 850 hPa (**a**) and 300 hPa (**b**).

The propagation path of quasi-biweekly cyclones during the $PM_{2.5}$ QBWO process for different types of events and their relationship to basic flow and barotropic energy conversion are shown in Figure 10. For $PM_{2.5}$-QBWO1 (Figure 10a), there is a westerly anomaly in the propagation path. Although there is an obvious positive center of barotropic energy conversion in South China, there is an obvious southeast wind anomaly south of the quasi-biweekly cyclone, which prevents the cyclone from moving southward. For the $PM_{2.5}$-QBWO2 events (Figure 10b), the quasi-biweekly cyclone originating near the Caspian Sea moves to the northeast under the influence of westerly and southwesterly anomalies. Different from the $PM_{2.5}$-QBWO1 events, there is no obvious background wind anomaly on the southeast side of Baikal Lake at this time, and disturbances in South China derive energy from the basic airflow, thereby splitting up a new cyclone in South China. The quasi-biweekly cyclone of the $PM_{2.5}$-QBWO3 events originates from higher latitudes, and it can be seen that the propagation path of the quasi-biweekly cyclone is consistent with the background wind anomaly (Figure 10c). For the $PM_{2.5}$-QBWO4 event (Figure 10d), the quasi-biweekly cyclone originating in the northern Aleutian region

propagates westward under the influence of easterly anomalies at high latitudes, and converges with the westward propagating quasi-biweekly cyclone originating in the Ural Mountains on the northwest side of Lake Baikal before propagating southward. The above analysis shows that in mid–high latitudes, the different propagating paths of quasi-biweekly cyclones are closely related to the basic airflow anomalies; The southward propagation of quasi-biweekly cyclones is due to the disturbance development in South China, where there is no significant anomaly in the background wind or the background wind is a northerly wind anomaly. The disturbance obtains energy from the basic airflow, which attracts the quasi-biweekly cyclone in high latitudes to move southward.

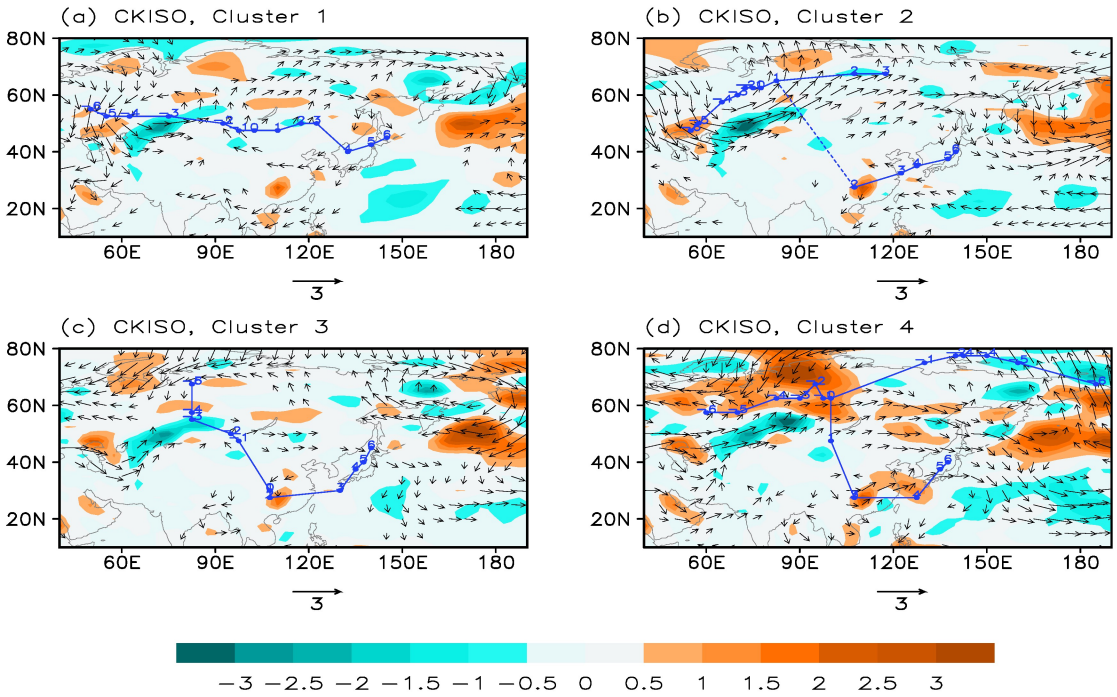

Figure 10. The 850 hPa basic flow anomaly (vector, unit: m/s) and barotropic energy conversion (shadow, unit: m^2/s^3) during the occurrence of $PM_{2.5}$-QBWO events (averaged from day −6 to day 6). (**a**–**d**) represent $PM_{2.5}$-QBWO1–4, respectively. The blue line in the figure represents the propagation path of the quasi-biweekly cyclone, and the blue number represents leading–lagging days. The blue dotted line in (**b**) indicates a center split from the cyclone at mid–high latitudes.

4. Discussion

Using daily high-resolution $PM_{2.5}$ data in China, combined with NCEP/NCAR reanalysis data, the sub-seasonal variation characteristics of $PM_{2.5}$ in North China and its leading circulation patterns in the winters from 1960/61 to 2019/20 were analyzed. It was found that there was a dominant period of 10–20 days of winter $PM_{2.5}$ in North China, which is consistent with the research results obtained by Liu et al. [29] and Gao et al. [30] based on observations of $PM_{2.5}$ after 2000. After the 1960s, as the concentration of $PM_{2.5}$ gradually increased, its quasi-biweekly oscillation frequency showed an increasing trend, and slightly weakened after 2014. Other studies [33] have also highlighted the characteristics of a decrease in $PM_{2.5}$ concentration after 2010. In addition, observed AOD data from AERONET stations were used to verify the credibility of $PM_{2.5}$ gridded data. During $PM_{2.5}$ oscillation, the AOD (440 nm band) also exhibited oscillation characteristics consistent with $PM_{2.5}$.

Persistent strong pollution occurs at the active period of $PM_{2.5}$ QBWO, while the air quality is good at the inactive stage. In the active phase of $PM_{2.5}$ QBWO, the Mongolian anti-cyclone is located in a west–north direction compared to the climatic state, far away from North China. North China is located in front of the abnormal cyclone. The abnormal southerly wind weakens the northerly wind, enhances the relative humidity, and sharply increases the concentration of $PM_{2.5}$. In the mid–high latitude regions, there are obvious

quasi-biweekly wave trains at both 850 hPa and 300 hPa. The recent research results [29–32] also indicate a close relationship between the $PM_{2.5}$ concentration and the Rossby wave train at mid–high latitudes.

In the study of Wu et al. [32], it was found that the QBWO of haze events in the Beijing–Tianjin–Hebei region in the winter of 1979–2013 in China was mainly influenced by the Rossby wave spreading eastward along the Eurasian continent from the North Atlantic Ocean. The peak phase of haze pollution was related to the zonal dipole, that is, the abnormal cyclone in the northwest of Lake Baikal and the abnormal anti-cyclone in the northeast of China and Japan. We further used the K-means clustering method to classify the 850 hPa circulation evolution during the $PM_{2.5}$ oscillation, and found that the quasi-biweekly circulation evolution during $PM_{2.5}$ QBWO can be classified into four types: eastward propagating events (EP, $PM_{2.5}$-QBWO1), eastward propagating and splitting events (EP-S, $PM_{2.5}$-QBWO2), southeast propagating events (SEP, $PM_{2.5}$-QBWO3), and combined and southward propagating events (CSP, $PM_{2.5}$-QBWO4). Among them, the EP events occurred more frequently in the 2010s and 2000s, and the EP-S events were more evenly distributed in the period of 1990–2010. It is worth mentioning that in the 1970s, most of the $PM_{2.5}$-QBWO events belonged to EP-S. SEP events were more common in the 1980s and 2000s, while the CSP events mainly occurred in the 1980s. This result highlights the diversity of intra-seasonal circulation patterns in the mid–high latitudes during the $PM_{2.5}$ QBWO over a longer time range, which is a powerful supplement to previous research.

In the active phases of the four types of $PM_{2.5}$ QBWO, North China exhibits a quasi- biweekly southerly anomaly, weakening wind speed and increasing humidity, and pollutants more likely to accumulate under the calm and humid conditions [4].

Finally, we explored the propagation mechanisms of different types of circulation. It was found that there are westerly anomalies in the propagation path of the quasi-biweekly cyclone in the low troposphere for the EP event, with southeast wind anomalies on the south side. There are southwest wind anomalies in the propagation path of the EP-S event. There are northerly anomalies in the source area of the SEP event, and in the CSP event, the quasi-biweekly cyclone in the northern part of Aleutian moves westward under the guidance of obvious easterly anomalies in high latitudes, and merges with the cyclone moving eastward from the Urals. Therefore, the different propagation paths of quasi-biweekly cyclones that affect $PM_{2.5}$-QBWO are significantly affected by basic flow anomalies, especially in the mid–high latitudes. In addition, in the lower troposphere, quasi-biweekly disturbances in South China can derive energy from the basic flow and then develop, which guides the quasi-biweekly cyclones in EP-S, SEP, and CSP events to reach South China. We also analyzed the circulations in the mid–high troposphere and found that they have similar characteristics, but the wave train is more northward than that at 850 hPa. This is the result of the mean north wind in the upper troposphere being weak, and at the same time, the energy conversion from the basic flow to quasi-biweekly disturbances being weak in the upper troposphere. Therefore, when studying the mechanism of $PM_{2.5}$ QBWO in eastern China, emphasis should be placed on the analysis of the lower troposphere first.

It also needs to be highlighted that, although this study has analyzed the process of $PM_{2.5}$ QBWO in North China caused by different leading circulation patterns in mid–high latitudes and explained the propagation mechanism of low-frequency wave trains, the existing research cannot better explain why the leading circulation patterns are different in different decades. This is very meaningful and will be the focus of our future research.

Author Contributions: Conceptualization, X.Z. and C.Y.; methodology, X.Z.; software, X.Z.; validation, C.Y.; formal analysis, X.Z.; investigation, X.Z.; resources, X.Z.; data curation, X.Z.; writing—original draft preparation, X.Z.; writing—review and editing, C.Y.; visualization, C.Y.; supervision, X.Z.; project administration, X.Z.; funding acquisition, X.Z. All authors have read and agreed to the published version of the manuscript.

Funding: This research was funded by the Key Projects of the National Natural Science Foundation of China, grant number 42030612, and special funds for the basic scientific research business expenses of the central level public welfare research institutes, grant number GYZX210501.

Institutional Review Board Statement: Not applicable.

Informed Consent Statement: Not applicable.

Data Availability Statement: Not applicable.

Acknowledgments: We thank Zhang Xiaoye and Zhao Tianliang for providing $PM_{2.5}$ gridded data. We also thank professor Hongbin Chen and Philippe Goloub (AERONET, PI for Beijing) for their efforts in establishing and maintaining the data in https://aeronet.gsfc.nasa.gov/new_web/download_all_v3_aod.html (accessed on 10 August 2022).

Conflicts of Interest: The authors declare no conflict of interest.

References

1. Dall'Osto, M.; Querol, X.; Alastuey, A.; O'Dowd, C.; Harrison, R.M.; Wenger, J.; Gómez-Moreno, F.J. On the spatial distribution and evolution of ultrafine particles in Barcelona. *Atmos. Meas. Tech.* **2013**, *13*, 741–759. [CrossRef]
2. Minguillon, M.C.; Querol, X.; Baltensperger, U.; Prévôt, A.S. Fine and coarse PM composition and sources in rural and urban sites in Switzerland: Local or regional pollution? *Sci. Total Environ.* **2012**, *427*, 191–202. [CrossRef] [PubMed]
3. Roy, D.; Singh, G.; Yadav, P. Identification and elucidation of anthropogenic source contribution in PM10 pollutant: Insight gain from dispersion and receptor models. *J. Environ. Sci.* **2016**, *48*, 69–78. [CrossRef]
4. Giemsa, E.; Soentgen, J.; Kusch, T.; Beck, C.; Münkel, C.; Cyrys, J.; Pitz, M. Influence of Local Sources and Meteorological Parameters on the Spatial and Temporal Distribution of Ultrafine Particles in Augsburg, Germany. *Front. Environ. Sci.* **2021**, *8*, 609846. [CrossRef]
5. Tao, Y.; Liu, Y.; Mi, S. Atmospheric pollution characteristics of fine particles and their effects on human health. *Acta Sci. Circumstantiae* **2014**, *34*, 592–597.
6. Akimoto, H. Global air quality and pollution. *Science* **2003**, *302*, 1716–1719. [CrossRef]
7. Wang, J.; Ogawa, S. Effects of meteorological conditions on $PM_{2.5}$ concentrations in Nagasaki, Japan. *Int. J. Environ. Res. Public Health* **2015**, *12*, 9089–9101. [CrossRef]
8. Wu, X.; Vu, T.V.; Shi, Z.; Harrison, R.M.; Liu, D.; Cen, K. Characterization and source apportionment of carbonaceous $PM_{2.5}$ particles in China—A review. *Atmos. Environ.* **2018**, *189*, 187–212. [CrossRef]
9. Cai, W.; Li, K.; Liao, H.; Wang, H.; Wu, L. Weather conditions conducive to Beijing severe haze more frequent under climate change. *Nat. Clim. Chang.* **2017**, *7*, 257–262. [CrossRef]
10. Chen, Z.; Chen, D.; Zhao, C.; Kwan, M.; Cai, J.; Zhuang, Y.; Zhao, B.; Wang, X.; Chen, B.; Yang, J. Influence of meteorological conditions on PM2. 5 concentrations across China: A review of methodology and mechanism. *Environ. Int.* **2020**, *139*, 105558. [CrossRef]
11. Zhang, L.; Wang, T.; Lv, M.; Zhang, Q. On the severe haze in Beijing during January 2013: Unraveling the effects of meteorological anomalies with WRF-Chem. *Atmos. Environ.* **2015**, *104*, 11–21. [CrossRef]
12. Andersson, A.; Deng, J.; Du, K.; Zheng, M.; Yan, C.; Skold, M.; Gustafsson, O. Regionally-Varying Combustion Sources of the January 2013 Severe Haze Events over Eastern China. *Environ. Sci. Technol.* **2015**, *49*, 2038–2043. [CrossRef] [PubMed]
13. Zhang, Z.Y.; Xu, X.D.; Qiao, L.; Gond, D.Y.; Kim, S.; Wang, Y.; Mao, R. Numerical simulations of the effects of regional topography on haze pollution in Beijing. *Sci. Rep.* **2018**, *8*, 5504. [CrossRef] [PubMed]
14. Guo, S.; Hu, M.; Zamora, M.L.; Peng, J.; Shang, D.; Zheng, J.; Du, Z.; Wu, Z.; Shao, M.; Zeng, L.; et al. Elucidating severe urban haze formation in China. *Proc. Natl. Acad. Sci. USA* **2014**, *111*, 17373–17378. [CrossRef]
15. Dang, R.J.; Liao, H. Severe winter haze days in the BeijingTianjin-Hebei region from 1985 to 2017 and the roles of anthropogenic emissions and meteorology. *Atmos. Chem. Phys.* **2019**, *19*, 10801–10816. [CrossRef]
16. Chen, D.L.; Liao, H.; Yang, Y.; Che, L.; Wang, H.L. Simulated aging processes of black carbon and its impact during a severe winter haze event inthe Beijing-Tianjin-Hebei region. *Sci. Total Environ.* **2021**, *755*, 142712. [CrossRef] [PubMed]
17. Wang, Y.; Yao, L.; Wang, L.; Liu, Z.; Ji, D.; Tang, G.; Zhang, J.; Sun, Y.; Hu, B.; Xin, J. Mechanism for the formation of the January 2013 heavy haze pollution episode over central and eastern China. *Sci. China Earth Sci.* **2014**, *57*, 14–25. [CrossRef]
18. Wang, Y.; Wang, L.; Zhao, G.; Wang, Y.; An, J.; Liu, Z.; Tang, G. Analysis of different-scales circulation patterns and boundary layer structure of $PM_{2.5}$ heavy pollutions in Beijing during winter. *Clim. Environ. Res.* **2014**, *19*, 173–184. (In Chinese)
19. Yin, Z.; Wang, H. Role of atmospheric circulations in haze pollution in December 2016. *Atmos. Chem. Phys.* **2017**, *17*, 11673–11681. [CrossRef]
20. Zhong, W.; Yin, Z.; Wang, H. The relationship between anticyclonic anomalies in northeastern Asia and severe haze in the Beijing–Tianjin–Hebei region. *Atmos. Chem. Phys.* **2019**, *19*, 5941–5957. [CrossRef]
21. Yin, Z.; Wang, H.; Chen, H. Understanding severe winter haze events in the North China Plain in 2014: Roles of climate anomalies. *Atmos. Chem. Phys.* **2017**, *17*, 1641–1651. [CrossRef]

22. Wang, L.; Zhang, N.; Liu, Z.; Sun, Y.; Ji, D.; Wang, Y. The influence of climate factors, meteorological conditions, and boundary-layer structure on severe haze pollution in the Beijing-Tianjin-Hebei region during January 2013. *Adv. Meteorol.* **2014**, *7*, 685971. [CrossRef]
23. Zhang, S.; Zeng, G.; Wang, T.; Yang, X.; Iyakaremye, V. Three dominant synoptic atmospheric circulation patterns influencing severe winter haze in eastern China. *Atmos. Chem. Phys.* **2022**, *22*, 16017–16030. [CrossRef]
24. Shen, L.; Jacob, D.J.; Mickley, L.J.; Wang, Y.; Zhang, Q. Insignificant effect of climate change on winter haze pollution in Beijing. *Atmos. Chem. Phys.* **2018**, *18*, 17489–17496. [CrossRef]
25. Li, M.; Chen, F.; Gan, Q.; Li, J.; Jiang, S.; Cao, J.; Zeng, D.; Huan, C.; Fan, S. Variation Characteristics of Particular Matter Concentration and Typical Pollution Processes During 2013–2016 in Huizhou City. *Meteorol. Environ. Sci.* **2019**, *42*, 89–96.
26. Shi, S.; Liu, Z.; Xu, Z.; Yang, S.; Liu, J.; Wang, Y. Evolution and meteorological causes of fine particulate explosive growth events in Beijing, China, from 2013 to 2017. *Atmos. Ocean. Sci. Lett.* **2020**, *13*, 55–62. [CrossRef]
27. Yao, S.; Sun, Q.; Huang, Q.; Zhang, C. The 10–30-day intraseasonal variation of the East Asian winter monsoon: The temperature mode. *Dyn. Atmos. Ocean.* **2016**, *75*, 91–101. [CrossRef]
28. Jiao, Y.; Wu, R.; Song, L. Individual and Combined Impacts of Two Eurasian Wave Trains on Intraseasonal East Asian Winter Monsoon Variability. *J. Geophys. Res. Atmos.* **2019**, *124*, 4530–4548. [CrossRef]
29. Liu, J.; Huang, W.; Zhang, Q. The quasi-biweekly oscillation of eastern China PM_(2.5) in response to different Rossby wave trains over the Eurasian continent. *Atmos. Res.* **2022**, *267*, 105990. [CrossRef]
30. Gao, L.; Wang, T.; Ren, X.; Zhuang, B.; Li, S.; Yao, R.; Yang, X. Impact of atmospheric quasi-biweekly oscillation on the persistent heavy $PM_{2.5}$ pollution over Beijing-Tianjin-Hebei region, China during winter. *Atmos. Res.* **2020**, *242*, 105017. [CrossRef]
31. Gao, L.; Wang, T.; Ren, X.; Ma, D.; Qu, Y.; Wu, H. Mechanism of persistent heavy $PM_{2.5}$ pollution over the Beijing-Tianjin-Hebei region of China: A combination of aerosol radiative effect and atmospheric quasi-biweekly oscillation. *Atmos. Environ.* **2023**, *303*, 119751. [CrossRef]
32. Wu, D.; Zhao, S.; Li, J.; Wang, W. Influences of atmospheric intraseasonal oscillation in mid–high latitudes on winter haze pollution over the Beijing-Tianjin-Hebei region. *Int. J. Climatol.* **2023**, *43*, 3173–3188. [CrossRef]
33. Zhong, J.; Zhang, X.; Gui, K.; Liao, J.; Fei, Y.; Jiang, L.; Guo, L.; Liu, L.; Che, H.; Wang, Y.; et al. Reconstructing 6-hourly $PM_{2.5}$ datasets from 1960 to 2020 in China. *Earth Syst. Sci. Data* **2022**, *14*, 3197–3211. [CrossRef]
34. Dai, Y.; Zhang, G.; Wei, X. Overview of the use of AERONET site data in China. *Sci. Technol. Innov. Guide* **2018**, *15*, 153–156. (In Chinese)
35. Wang, J.; Zhu, C.; Zhu, Y.; Chen, S.G. Correlation between remote sensing aerosol parameters and $PM_{2.5}$ in Beijing. *China Environ. Sci.* **2015**, *35*, 1947–1956. (In Chinese)
36. Ying, C.; Ge, B.; Hao, S.; Xu, H.; Liu, Y.; Gan, L.; Wang, Z. Inversion of $PM_{2.5}$ Concentration in Beijing Based on Visibility and AOD Data. *Clim. Environ. Res.* **2020**, *25*, 521–530. (In Chinese)
37. Kalnay, E.; Kanamitsu, M.; Kistler, R.; Collins, W.; Deaven, D.; Gandin, L.; Iredell, M.; Saha, S.; Whilte, G.; Woollen, J. The NCEP/NCAR 40-year reanalysis project. *Bull. Am. Meteor. Soc.* **1996**, *77*, 437–470. [CrossRef]
38. Kaufman, L.; Rousseeuw, P.J. *Finding Groups in Data: An Introduction to Cluster Analysis*; John Wiley & Sons: Hoboken, NJ, USA, 2009.
39. Wang, B.; Chen, G.; Liu, F. Diversity of the Madden-Julian oscillation. *Sci. Adv.* **2019**, *5*, eaax0220. [CrossRef]
40. Wang, L.; Jiang, J.; Li, T.; Zhou, X.; Chen, Z. Three distinct circulation patterns that induce enhanced intraseasonal precipitation events over South China in boreal winter. *Clim. Dyn.* **2022**, *60*, 2893–2905. [CrossRef]
41. Takaya, K.; Nakamura, H. A formulation of a wave-activity flux for stationary Rossby waves on a zonally varying basic flow. *Geophys. Res. Lett.* **1997**, *24*, 2985–2988. [CrossRef]
42. Takaya, K.; Nakamura, H. A formulation of a phase-independent wave-activity flux for stationary and migratory quasigeostrophic eddies on a zonally varying basic flow. *J. Atmos. Sci.* **2001**, *58*, 608–627. [CrossRef]
43. Cai, M.; Yang, S.; Dool, H.; Kousky, V. Dynamical implications of the orientation of atmospheric eddies: A local energetics perspective. *Tellus Ser. A-Dyn. Meteorol. Oceanogr.* **2007**, *59*, 127–140. [CrossRef]
44. Wang, X.; Zhang, R.; Tan, Y.; Yu, W. Dominant synoptic patterns associated with the decay process of $PM_{2.5}$ pollution episodes around Beijing. *Atmos. Chem. Phys.* **2020**, *21*, 2491–2508. [CrossRef]
45. Liu, Y.; Wang, B.; Zhu, Q.; Luo, R.; Wu, C.; Jia, R. Dominant Synoptic Patterns and Their Relationships with $PM_{2.5}$ Pollution in Winter over the Beijing-Tianjin-Hebei and Yangtze River Delta Regions in China. *J. Meteorol. Res.* **2019**, *33*, 765–776. [CrossRef]
46. Carillo, A.; Ruti, P.M.; Navarra, A. Storm tracks and zonal mean flow variability: A comparison between observed and simulated data. *Clim. Dyn.* **2000**, *16*, 219–228. [CrossRef]
47. Nakamura, H.; Izumi, T.; Sampe, T. Interannual and decadal modulations recently observed in the Pacific storm track activity and east Asian winter monsoon. *J. Clim.* **2002**, *15*, 1855–1874. [CrossRef]